Particle
& Particle Systems Characterization
www.particle-journal.com

Carbon-Dot-Decorated Nanodiamonds

Olga Shenderova, Suzanne Hens, Igor Vlasov, Stuart Turner, Ying-Gang Lu, Gustaaf Van Tendeloo, Amanda Schrand, Sergey A. Burikov, and Tatiana A. Dolenko*

The synthesis of a new class of fluorescent carbon nanomaterials, carbon-dot-decorated nanodiamonds (CDD-ND), is reported. These CDD-NDs are produced by specific acid treatment of detonation soot, forming tiny rounded sp^2 carbon species (carbon dots), 1–2 atomic layers thick and 1–2 nm in size, covalently attached to the surface of the detonation diamond nanoparticles. A combination of nanodiamonds bonded with a graphitic phase as a starting material and the application of graphite intercalated acids for oxidation of the graphitic carbon is necessary for the successful production of CDD-ND. The CDD-ND photoluminescence (PL) is stable, 20 times more intense than the intrinsic PL of well-purified NDs and can be tailored by changing the oxidation process parameters. Carbon-dot-decorated DNDs are shown to be excellent probes for bioimaging applications and inexpensive additives for PL nanocomposites.

1. Introduction

The rapid advancement in nanomaterial fabrication has brought a broad plethora of fluorescent nanoparticles, which are indispensable for bioimaging applications in life sciences,[1] optoelectronic applications including light-emitting devices and display backlighting, photovoltaic, and photodetector devices, anti-counterfeiting products, airborne pollution sensors, and even quantum information processing.[2] Quantum dots made from group II–VI and III–V semiconductor materials, typically 2–10 nm in size, are the most popular fluorescent nanoparticles for these applications due to their high brightness, spectral tunability, narrow emission spectra, and photostability.[3] However, cadmium and other heavy metals used in conventional group II–VI quantum dots are a major concern in commercial applications.[2,4] In addition, in bioimaging applications, blinking effects in quantum dots prevent reliable long-term single particle tracking.[5] Recent reports show that blinking can be reduced or even suppressed,[6] but at the expense of a higher bleaching yield.[7] Blinking and toxicity of quantum dots motivate investigation of alternative materials. Alternative inorganic fluorescent nanocrystals include group IV nanoparticles (silicon, silicon-carbide, diamond, and germanium),[8] core–shell fluorescent silica nanoparticles, lanthanide-doped oxide, and other oxide nanoparticles.[1,9] Photoluminescent (PL) metal nanoparticles and clusters (Au, Ag, Cu, Pt, and others) have also been fabricated recently.[10,11]

Important requirements for PL nanoparticles in biological applications include low toxicity of the particles and high quantum yield and photostability of their luminescence. Because of their innate biocompatibility, high resistance against photobleaching, long fluorescence lifetime and wide fluorescence spectral region, carbon-based nanomaterials are gradually evolving into bioimaging probes of a new generation, also providing a drug carrier capability.[12–14]

There are several categories of carbon-based luminescent nanoparticles. The first group are so-called carbon dots, which are small, surface-passivated carbon nanoparticles with a particle size below 10 nm and fluorescence that most likely originates from surface energy trapping sites and their associated radiative recombinations. In order to ensure bright fluorescence emission, a very large surface-to-volume ratio for carbon dots is required.[15] Various carbon-based starting materials, such as soot, activated carbons, graphite, carbohydrates,[12–14] and nanodiamond[16] have been used as precursors to luminescent carbon-based nanomaterials using oxidizing conditions at elevated temperatures. Surface-passivated carbon dots are strongly emissive in the visible region, and emission intensity typically peaks in the green, sometimes extending into the near-infrared (NIR) region.[12,14] Carbon dots exhibit no optical blinking[15] and are highly photochemically stable with experimentally

Dr. O. Shenderova, Dr. S. Hens
International Technology Centre
8100-120 Brownleigh Drive, Raleigh, NC 27617, USA
E-mail: oshenderova@itc-inc.org
Dr. I. Vlasov
General Physics Institute
Russian Academy of Sciences
38 Vavilov Street, 119991 Moscow, Russia
Dr. S. Turner, Y.-G. Lu, Prof. G. V. Tendeloo
EMAT, University of Antwerp
Groenenborgerlaan 171, 2020 Antwerp, Belgium
Dr. A. Schrand
Applied Biotechnology Branch
Human Effectiveness Directorate, AFRL/RHPB
2729 R Street, Bldg 837, Wright-Patterson AFB, OH 45433-5707, USA
Dr. S. A. Burikov, Dr. T. A. Dolenko
Physical Department
Moscow State University
Leninskie Gory, 119991 Moscow, Russia

DOI: 10.1002/ppsc.201300251

determined emission quantum yields up to 75%.[17] According to in vitro and in vivo biological evaluations, carbon dots are non-toxic.[12,14]

A second large group of fluorescent carbon-based structures is related to graphene oxide (GO). The atomic structure of GO is composed of a graphene basal plane with a non-uniform coverage of oxygen-containing functional groups, such as epoxy and hydroxyl groups, resulting in sp^2 carbon islands of a few nanometers in size isolated within a defective sp^3 carbon network. Edges of the GO can contain other various oxygen-containing groups.[12–14] Typical C:O ratios in GO range between 2 and 4. Although luminescent GO structures can be relatively large, isolated structures of nanometer size can be also produced (nanoGO).[18,19] A popular method of the production of PL GO-based structures is the creation of nanosized sp^2 islands by a partial reduction of graphite oxide. The latter is typically obtained by oxidizing graphite under harsh conditions (Hummers and modified Hummers methods), followed by exfoliation into predominantly single-layer sheets. The fluorescence for GO-based structures has been reported from the visible to the NIR range and the maximum intensity is located between 500 and 800 nm.[12–14] Photoluminescence in GO-based structures was proposed to originate from emissive electronic transitions within a bandgap formed by quantum confinement in the isolated sp^2 carbon islands,[20] as well as by functionalized surface defect sites.[20–22] The use of PL nanoGO in biological imaging was demonstrated both in vivo and in vitro.[12–14] Although passivated carbon dots and nanoGO particles demonstrate bright stable luminescence, PL nanocarbons obtained by different chemical treatments vary widely in structure and composition as well as their PL properties. "Standardization" of the produced PL nanocarbons would be very useful for future advancement of their applications in bioimaging.

A third large group of fluorescent carbon nanostructures is based on nanodiamond (ND) particles. Nanodiamond particles are produced by detonation of carbon-containing explosives (DND) or by grinding of microdiamond powders manufactured by static high-pressure, high-temperature (HPHT) synthesis.[23] These two classes of ND particles have different structural characteristics and, as a result, different optical properties. A major difference between DND and HPHT ND in terms of optical applications is the state and content of nitrogen impurities within the core of the ND particles. NDs of HPHT synthesis contain N as a natural impurity in the form of the substitutional nitrogen (Ns) with concentrations of up to 300 ppm (for HPHT ND type Ib). ND produced from natural diamond type Ia (Ns concentration up to 3000 ppm) is also available. High-energy particle irradiation of type Ib ND followed by annealing causes formation of PL NV centers with red emission,[24] while ND from diamond Ia demonstrates green luminescence originating from the formation of N-V-N centers after irradiation and annealing.[25] Diamond nanoparticles containing NV color centers have caught on as an attractive alternative to quantum dots with stable luminescence that does not photobleach or photoblink.[26] The emission from NV defects peaks in the red and NIR spectral regions and is therefore attractive for biological labeling. Additionally, improved intracellular contrast may be achieved by time-gated imaging, taking advantage of the long decay lifetime (20 ns) of PL ND[27] as compared to the short decay lifetime of the cell medium auto fluorescence (2 ns). The first report of the use of PL NDs for biological labeling appeared in 2005,[26] demonstrating that PL-NDs containing NV centers are spontaneously internalized in HeLa cells and show the absence of toxicity in in vitro experiments. Many reports indicate the spontaneous internalization and efficient detection of PL NDs in cells during in vivo imaging as well.[28] Production of HPHT nanodiamonds with sizes smaller than 35 nm, containing a sufficient number of NV centers to provide the required brightness for inter-cell imaging, though, is still challenging. Up to now, nanodiamonds synthesized from explosives were not among the preferred candidates for imaging applications.[29] Although DND contains up to 2–3 wt% of N, the N conglomerates in DND are mainly optically inactive.[30] Advantages of DND include the small size of the primary particles (≈1–6 nm)[31] and available industrial production resulting in 1–2 orders of magnitude less expensive material than HPHT ND. DND has a low level of intrinsic photoluminescence,[29,30] related to residual sp^2 carbon phase present in the DND; however, surface modification can provide DND with PL properties.[32,33] Thus, synthesis of NDs a few nanometers in size with bright red luminescence for biological imaging remains an important goal.

In this paper, we report that specific acid treatment of ND-containing detonation soot, produces tiny rounded sp^2 carbon species (carbon dots), which are 1–2 atomic layers thick and covalently attached to the surface of DND particles. These carbon-dot-decorated DNDs demonstrate stable red PL that exceeds the PL intensity of typical DND by more than a factor of 20 and can be tailored by changing the oxidation process parameters. As DNDs can be de-agglomerated into individual ≈5 nm primary particles or fractionated to small size aggregates, this approach provides perspectives for the production of sub-10 nm size PL NDs with bright stable luminescence in the red and NIR regions, which is extremely well suited for biological imaging. The simplicity and effectiveness of the treatment of the detonation soot with graphite intercalated (GIC) acids for the production of CDD-ND holds promise for large-scale production of inexpensive PL ND.

2. Results

Recently, we demonstrated that a 3:1 sulfuric to nitric acid mixture can be used to produce PL nanostructures by oxidation of micrographite, nanographite, and other graphitic source materials at temperatures exceeding 100 °C.[34–36] It was possible to control the PL color of the reaction suspension by tuning the reaction temperature and/or reaction time. Various graphite oxide nanostructures were observed in the reaction suspension with increasing reaction time, including nanoribbons, graphene-like nanoplatelets, and sub-10 nm nanoparticles. In this paper, a similar treatment was applied to detonation soot, which is a product of the detonation of carbon-containing high-energy explosives[23] and consists of a mixture of nanodiamond and graphitic carbon. A starting sample of detonation soot in the 3:1 sulfuric/nitric acid mixture has a characteristic black color owing to the presence of sp^2 carbon. A color change of the residue from black to gray in an oxidation reaction is typically

DOI: 10.1002/ppsc.201300251

assigned to the oxidation of the non-diamond carbon component in the soot, and production of a gray purified ND powder. During treatment of the soot in the 3:1 sulfuric to nitric acid mixture, oxidation of the non-diamond carbon in the soot takes place relatively quickly (within tens of minutes) when the temperature exceeds roughly 100 °C. In order for this quick oxidation to take place, the weight ratio of the detonation soot and the acid mixture should exceed approximately 1:100. Surprisingly, the gray colored NDs, washed from the acids after reaction, possess a bright luminescence, which is visible on a UV bench or under a fluorescent microscope. As was the case in a previous study,[35] oxidation of the sp^2 phase of the soot with the acid mixture results in the production of graphene/graphite oxides structures with bright orange PL. The details of this treatment are listed below.

2.1. Oxidation Treatment and Luminescence

In a series of experiments, detonation soot-1, containing ≈70 wt% of nanodiamond and 30% of graphitic carbon, was treated in similar conditions (amounts of reagents and duration of treatment), but at different temperatures: 70, 80, and 90 °C. The residue was carefully washed in DI water and inspected using a fluorescence microscope. Water suspensions of the residue were also inspected on a UV bench. It was concluded that treatment at approximately 80 °C and above is needed to produce structures containing PL ND. Within the temperature range of ≈80–100 °C, at least 2–3 h treatment is required to produce PL structures, while at higher temperatures, results of the soot oxidation become noticeable after a short treatment time (tens of minutes). Photographs of the acidic reaction media, containing oxidized soot products after a treatment of detonation soot-1 in a 3:1 sulfuric/nitric acid mixture at 115 °C for increasing reaction time intervals, are shown in Figure S1 (Supporting Information). From the set of samples illuminated with white light, it can be seen that the color of soot in the reaction media progresses from very dark gray (15 min of treatments), to light gray for treatments exceeding 75 min. The oxidized ND particles in Figure S1 (Supporting Information) are suspended in the acidic reaction media. The samples demonstrate orange–yellow PL with a grayish hint due to the nanodiamond particles, when illuminated with a 365 nm UV lamp (Figure S1, Supporting Information, bottom). If the reaction media are left undisturbed, the NDs sediment to the bottom, forming gray-white residues (color depends on the duration of the treatment). The transparent supernatant, free of nanodiamonds, has a light-yellow color in white light and very bright yellow-orange PL under UV illumination (Figure S2, Supporting Information). This color is characteristic of graphite/graphene oxide (GO) nanoparticles.[35] As will be shown below by transmission electron microscopy (TEM), the transparent yellow supernatant contains nanometer-sized carbon spheres (sp^2 carbon structures) from approximately 5 nm up to 10–20 nm in size.

The nanodiamond samples, obtained by the method presented here, will be called carbon-dot-decorated NDs (CDD-NDs), in accordance with their structure revealed below by high-resolution TEM (HRTEM). The term "dots" is attributed to single-digit sp^2 carbon structures, ranging from less than 1 nm to a few nanometers in size. The CDD-NDs were extracted from the acidic media by repeated washing in DI water using centrifugation and sonication. Every sample was washed until no free-standing carbon dots or balls were left in the supernatant after centrifugation. The zeta potential in DI water of the washed CDD-ND was between −35 and −45 mV, with an average volumetric particle size of 100 nm. Using centrifugation, the sample was separated into more narrow size fractions, including a fraction of 20–30 nm particles, which was used in the cell studies. After the collected CDD-ND were resuspended in DI water and placed on a bench under UV light, all samples demonstrated surprisingly strong pinkish-reddish photoluminescence (**Figure 1**). Samples treated in the acid mixture over 2–5 h visually exhibited the strongest PL.

PL spectra of dry powders of CDD-NDs treated for various time are shown in **Figure 2**. The integral PL intensities appeared to be 10 to 20 times stronger for the samples as compared to the well-purified DND (bottom line of the Figure 2a). It can also be concluded from Figure 2 that it is possible to maximize the PL emission by choosing the proper treatment time (at a fixed temperature). The maximum intensity of the emission was observed for a sample treated for 2 h at 115 °C. For the samples treated for 30, 45, and 60 min, the emission peak position remained at 660–680 nm when using an excitation wavelength of 488 nm (Figure 2a). For the reaction time of 90 min and 2 h, the emission peak was blue-shifted to approximately 620 nm. At the same time, emission in the region around 800 nm decreased (as compared to the sample treated

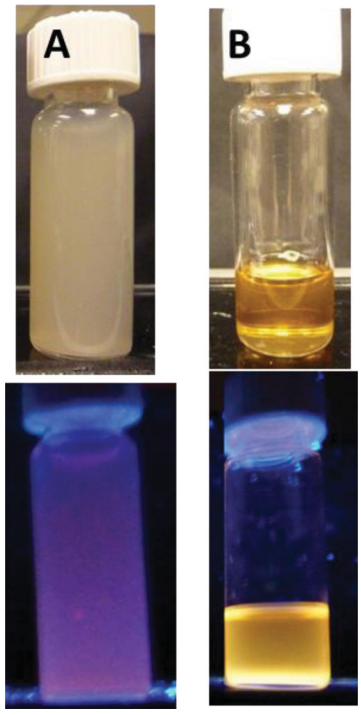

Figure 1. Photographs of the DI water suspension of CDD-ND A) and supernatant solution in the acids B) produced after 5 h of treatment of detonation soot-1 with a mixture of 3:1 sulfuric/nitric acid at 115 °C. The samples are illuminated with a white light (top) and 365 nm UV light (bottom).

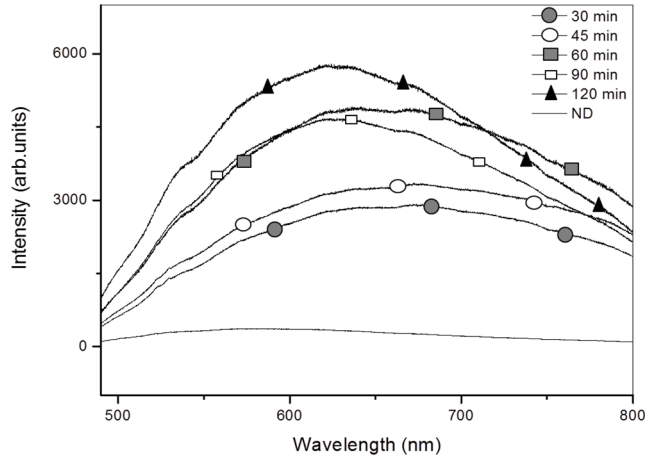

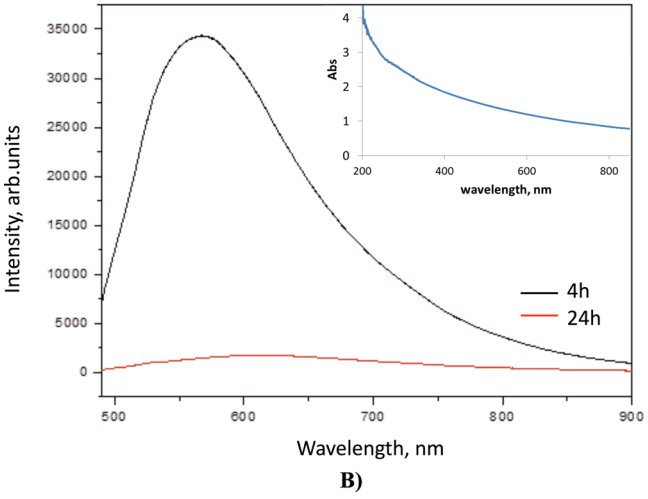

Figure 2. Fluorescence emission spectra measured for: A) typical detonation ND (bottom line) and for the CDD-ND produced at increasing reaction time by treatment of detonation soot-1 with a mixture of 3:1 sulfuric/nitric acids at 115 °C; B) CDD-ND produced by a 4 and 24 h treatment of detonation soot-2 in a mixture of 3:1 sulfuric/nitric acids at 115 °C. The excitation wavelength is 488 nm. (see also Figure S3, Supporting Information). The inset to Figure 2b shows absorption spectra of a 0.3 mg mL^{-1} CDD-ND suspension in DI water.

for 60 min). Absorption spectra of the CDD-ND did not reveal any characteristic peaks (Figure 2b).

The treatments described above for the sample soot-1 were repeated with a sample marked as soot-2. This sample was produced by a method of "dry synthesis", and contained only 35 wt% of ND and 65% of graphitic carbon in the soot, whereas sample soot-1 contained 70 wt% of ND owing to preservation of ND phase during fast "wet" cooling of the detonation products. After treatment of the sample soot-2 in a mixture of 3:1 sulfuric/nitric acid at 115 °C for 5 h and washing with DI water, its PL was also high (Figure S3, Supporting Information). Figure 2b demonstrates 20 times stronger PL intensity from the sample soot-2 treated for 4 h as compared to the sample soot-2 treated for 24 h (bottom line at the figure). It is also seen that the emission band of 4 h treated soot-2 has a clear pronounced maximum at 590 nm.

Importantly, higher temperature and longer time of treatment leads to essential decrease of the sample luminescence. For instance, in one of the experiments, soot-2 was treated at 130 °C and showed red PL for the washed CDD-ND from a probe taken after 1 h of treatment. The remaining sample in the acidic reaction media was additionally treated for 20 min at 200 °C. After the treatment, the residue appeared white. This white residue is a well-purified ND (as confirmed by Raman spectroscopy). Inspection of the washed residue in a fluorescent microscope did not reveal PL emission. In another experiment, soot-2 was treated for 24 h at 115 °C. The washed ND revealed very weak PL (Figure S3, Supporting Information and Figure 2b). These examples show that, in order to obtain intense photoluminescence for the treated samples, the reaction needs to be stopped before all sp^2 carbon has been fully oxidized.

In order to reveal the role of the starting material (soot) in the production of CDD-ND and to explore alternative ways of CDD-ND synthesis, a well-purified ND sample was boiled in the acid mixture together with independently produced carbon dots from nanographite.[35] The intention of this experiment was to attach CDs to NDs. After 2 h of the reaction time, followed by washing and extraction of NDs by centrifugation, the final ND sample demonstrated weak PL. It can then be concluded that during treatment in the acid mixture, chemisorption of free standing carbon dots does not take place and the use of detonation soot as a starting material is essential. In the soot, NDs and sp^2 carbon are covalently bonded and it can be assumed that a fraction of these bonds between the ND surface and the residual sp^2 carbon is preserved, forming carbon dots bonded to the ND surface.

To be able to judge the influence of the acid mixture (3:1 sulfuric/nitric acids ratio) on the final product, similar reactions were repeated with fuming nitric acid and 1:1 sulfuric/nitric acid mixtures. No visible oxidation of the soot was achieved, even at high temperature and over several hours of oxidative reaction.

In a series of experiments, other starting ND–graphitic carbon complexes were also tested. Polycrystalline diamond, produced from graphite by a shockwave-induced phase transformation typically contains inclusions of a graphitic phase, as confirmed in Raman and XRD measurements.[29] Treatment of the polycrystalline nanodiamond particles in the 3:1 sulfuric/nitric acids mixture produced a bright blue PL supernatant containing free carbon dots; well-washed diamond particles did not show appreciable PL. Similar results were obtained for detonation NDs with a high content of amorphous carbon. An experiment was also done with onion-like carbon structures containing ND cores, produced by a high temperature vacuum annealing of DNDs.[37] The supernatant consisting of free CDs showed bright orange PL. Well-washed ND demonstrated PL that was less bright compared to the CDD-ND produced from detonation soot.

In order to test the performance of CDD-NDs in biology-related media, the emission intensity of water slurries of CDD-ND was measured. These intensities were compared to the emission intensity of other nanocarbon-based PL particles, such as well-purified DND and graphene/graphite oxides

DOI: 10.1002/ppsc.201300251

produced by the acid oxidation of nanographite (Figure S4A, Supporting Information). An inset Table in Figure S4A (Supporting Information) contains the parameter F_o for all these samples. The parameter F_o is a quantitative characterization of the photoluminescence, being the ratio of integral intensity of photoluminescence to the integral intensity of the water Raman valence band.[38,39] The polydispersed CDD-ND sample, obtained after 90 min of acid treatment, has a 10 times higher intensity than a typical polydispersed ND. NanoGO has an almost 100 times higher brightness than CDD-ND particles (50 times in comparison with the most bright CDD-ND obtained after 2 h of treatment). Figure S4B (Supporting Information) illustrates the PL intensity stability of the suspensions, including a suspension of organic dye Alexa Fluor, under prolonged laser irradiation. All carbon-based samples demonstrate high stability of the PL, while the intensity of the Alexa sample decreased by 45%. Deviation from the average of the integral PL intensity was 3–4% for the CDD-ND and the nanoGO samples, and 6–8% for the well-purified DND samples.

2.2. Structural Characterization: Electron Microscopy, XRD, XPS

To better understand the processes involved in the carbon dots formation, the typical detonation soot prior to treatment and the graphitic material collected from the supernatant of the reaction media were investigated, and are displayed in **Figure 3**a,b. The HRTEM image of detonation soot in Figure 3a clearly shows that the starting material is a mixture of nanodiamond (white arrows) and graphitic structures (e.g., onion structures, indicated by black arrows). The inset Fourier transform pattern shows the presence of both graphitic and diamond lattice reflections, typical for this type of material. An image of the supernatant material is displayed in Figure 3b. This heavily agglomerated material is mainly amorphous, as evidenced by the lack of lattice reflections in the inset Fourier transform.

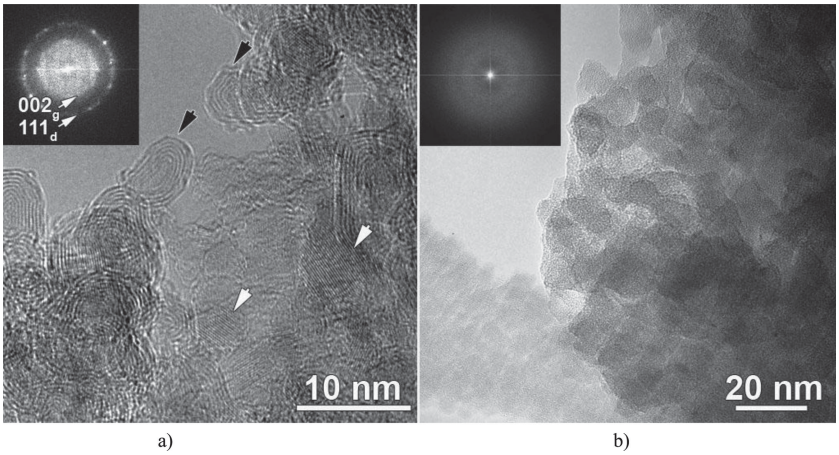

a) b)

Figure 3. TEM investigation of the detonation soot and carbon supernatant material. a) HRTEM image of detonation soot, a mixture of nanodiamond (white arrows) and graphitic material (e.g., onion-like structures, black arrows), the starting material for the production of carbon dot-decorated diamonds. The inset Fourier transform shows the presence of both graphitic and diamond lattice reflections. b) Heavily agglomerated carbon material collected from the supernatant of the reaction media. The material is mainly amorphous, as evidenced by the lack of lattice reflections in the inset Fourier transform.

HRTEM images of the carbon dot decorated DND material are displayed in **Figure 4**a–c. Figure 4a is an overview image of the material; the white arrows point to round graphitic structures and 1–2 nm carbon dots at the nanodiamond surfaces. These structures are clearly present all over the nanodiamond material surfaces. The inset electron diffraction pattern taken from the same region only displays lattice reflections typical of the diamond crystal structure, evidencing that all large graphitic onion structures have been destroyed. The HRTEM images in (b) and (c) show that the dots are attached to the nanodiamond surfaces. These nanodiamond surfaces are generally covered by 1–2 monolayers of graphitic material, which, in turn, is attached to the carbon dots. The inset Fourier transform in (c) evidences the diamond particle in the white rectangle is imaged along the [011] zone axis orientation.

The nature of the carbon dots was further investigated using spatially resolved electron energy-loss spectroscopy, performed in the same microscope as the HRTEM imaging but operated in scanning TEM (STEM) mode. To do so, we adopted the so-called spectrum imaging technique (Supporting Information). In this technique, the sample area of interest, here containing dots-decorated nanodiamonds (**Figure 5**a), is scanned in small steps using a fine (≈1.5 Å) electron probe. At each point of the scan, an EELS signal is acquired containing the C-K (285 eV), the N-K (400 eV), and the O-K (532 eV) edge, allowing the chemical nature of the material to be investigated. A dark-field STEM overview image, taken simultaneously with the 49*27 point spectrum image, is displayed in Figure 5a. Several nanometer-sized structures, presumably the carbon dots, are visible at the surface of the nanoparticles. Averaged EELS spectra from regions marked by 1 and 2 in Figure 5a are plotted in Figure 5e. The top EELS spectrum from region 1, a nanodiamond region, shows the presence of carbon at this position through the C-K edge starting at 285 eV, but also a small amount of nitrogen though the N-K edge around 400 eV. The fine structure of the C-K edge, with a large σ* contribution starting at 292 eV, corresponds largely to the diamond energy-loss near edge (ELNES) signature.[40] The small π* contribution at 285 eV in this spectrum arises from graphitic material at the top and bottom nanodiamond surfaces. An overview spectrum with high *S*/*N* ratio, summed over many CDD-ND particles simultaneously is displayed in Figure S5 (Supporting Information). Again, the π* contribution at 285 eV arises from the graphitic structures and dots at the ND surfaces, while the large σ* contribution at 292 eV confirms that the majority of the material is indeed still diamond. The nitrogen signal, peaking around 403 eV, mainly arises from nitrogen embedded within the nanodiamond cores.[41]

The spectrum from a single-carbon dot at the nanodiamond surface, spectrum 2, looks distinctly different from spectrum 1. The fine structure of the C-K edge has a large π* contribution at 285 eV, and a broader σ* contribution. The σ* contribution in the spectrum does not show the presence of sharply

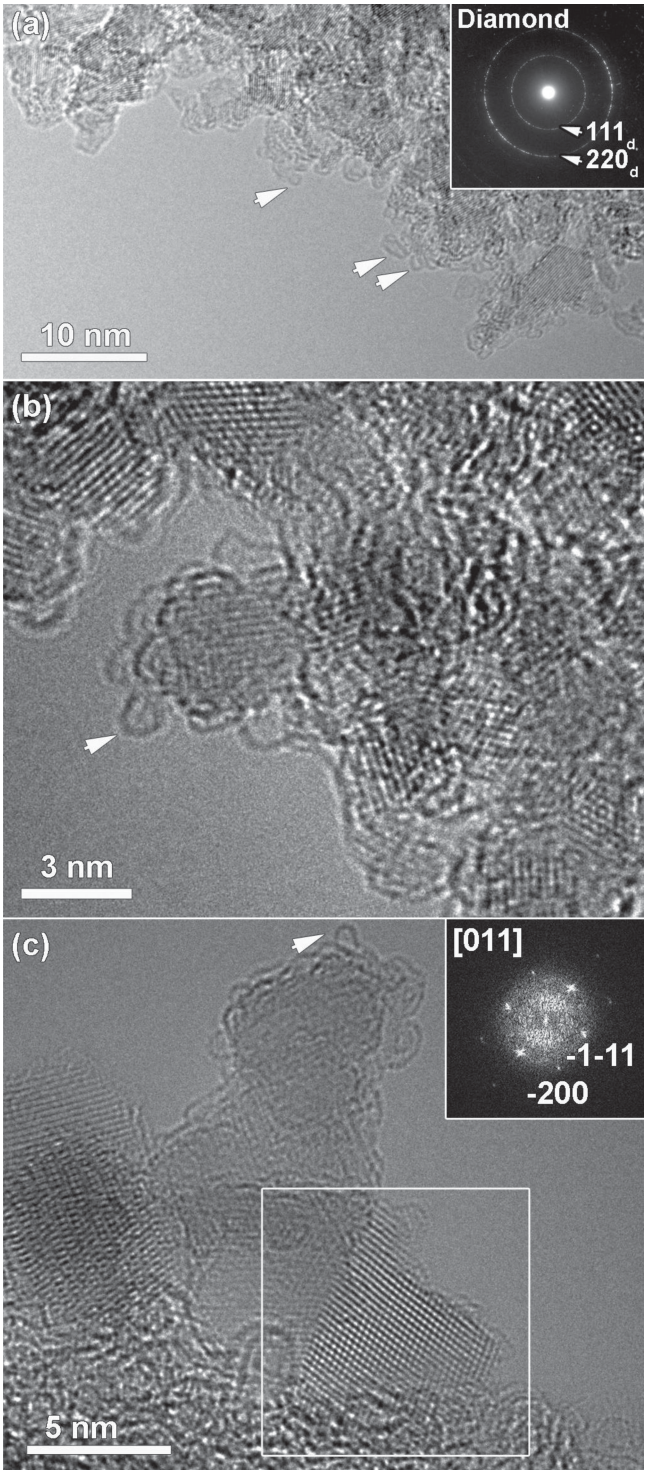

Figure 4. TEM investigation of CDD-ND. a) Overview image of typical CDD-ND material. The white arrows point to round graphitic structures and 1–2 nm carbon dots at the nanodiamond surfaces. The inset electron diffraction taken from a similar region only displays lattice reflections typical of the diamond crystal structure, evidencing that all large graphitic onion structures have been destroyed. b,c) High-resolution TEM images showing the dots are attached to the nanodiamond surfaces, which are generally covered by 1–2 monolayers of graphitic material. The inset Fourier transform in (c) evidences the diamond particle in the white rectangle is imaged along the [011] zone axis orientation.

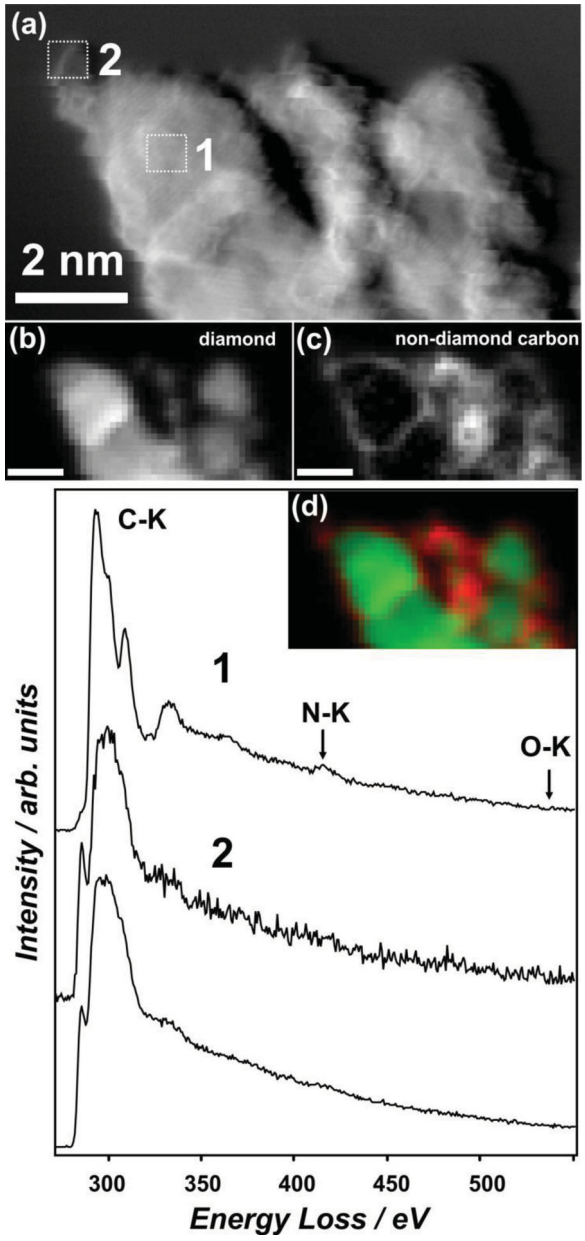

Figure 5. STEM-EELS investigation of CDD-ND. a) ADF-STEM overview image of the region investigated by spatially-resolved EELS. b) Diamond map. c) Non-diamond carbon map; the scale bar is 2 nm in (b) and (c). d) Color maps showing the non-diamond shell and dots covering the diamond nanoparticle cores. e) Extracted EELS spectra from regions 1 (nanodiamond) and region 2 (carbon dot) in the EELS spectrum image. The bottom spectrum is a summed spectrum from several dots.

defined peaks, as is the case for graphite, but also does not correspond to the case for amorphous carbon. As was clear from the HRTEM images, the dots are made up of graphitic material that is highly deformed or defected. No significant nitrogen or oxygen signal is detected in the carbon dot structure in position 1. As the signal to noise (S/N) ratio in the spectrum is relatively low, due to the small size of the carbon dot structure, an averaged spectrum from several dots is also plotted in Figure 5e. The spectrum confirms that no significant nitrogen or oxygen signal is present in the carbon dots.

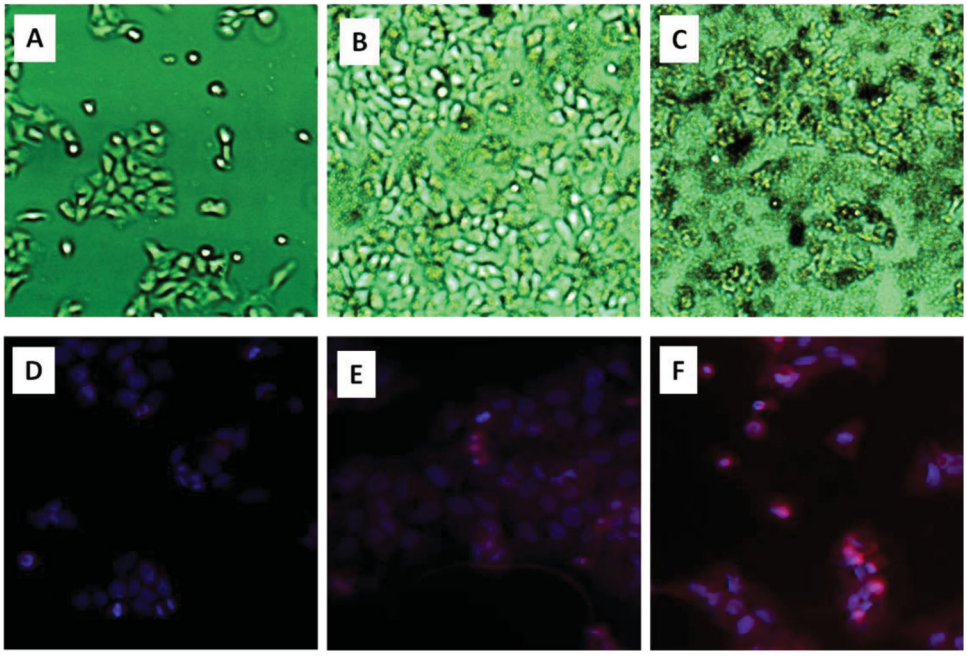

Figure 6. A–C) Representative transmitted light and D–F) fluorescent images of HaCat cells dosed with 25 μg mL^{-1} of nanodiamonds for 24 h. A,D) Control. B,E) Typical detonation ND. C,F) Carbon dots decorated ND. Nanodiamonds appear in red and nuclear counterstain in blue.

To plot the distribution of diamond and non-diamond carbon species in the studied region, we fitted a diamond reference as well as the reference obtained from several carbon dots to all the acquired spectra. Plotting the intensity of the two fitted components provides the diamond and non-diamond (graphitic material) maps displayed in Figure 5b,c. A color overlay of both is also plotted in Figure 5d.

XRD spectra of the CDD-ND produced by treatment of detonation soot-1 at 115 °C for different time intervals are shown in Figure S6 (Supporting Information). For the sample treated for 1 h, both diamond (≈46° (diamond (111) and 75°(diamond 220)) and graphite (≈27°) phases present, while in the sample treated for 4 h the diamond phase dominates. This illustrates that the small 1–2 nm carbon dots formed after several hours of treatment do not provide a noticeable contribution to the XRD graphite peak, confirming the HRTEM and ED results obtained above.

XPS spectra of the CDD-ND produced by treatment of detonation soot-1 at 115 °C for 4 h are shown in Figure S6 (Supporting Information). The spectra are typical for DND and have broad C 1s and O 1s peaks. Based on XPS measurements, the CDD-ND samples contain ≈6 wt% of oxygen, ≈2 wt% of nitrogen, and 92 wt% of carbon. FTIR spectra (not shown) demonstrate a well-pronounced 1730 cm^{-2} carbonyl peak which, in combination with negative zeta potential, confirms the presence of carboxylic groups on the CDD-ND surface.

2.3. Demonstrations of Applications

2.3.1. Cells Studies

CDD-ND agglomerates with an average particle size of about 20–30 nm were used in the cell studies. In parallel, well-purified detonation ND agglomerates with average sizes of 60–80 nm and weak surface structural luminescence (bottom graph at Figure 2a) were also investigated. HaCat cells incubated with or without nanodiamonds for 24 h displayed normal elongated morphologies (**Figure 6**B,C) compared to control cells (Figure 6A) as demonstrated with transmitted light microscopy. The difference in relative fluorescent intensity and uptake of the two different nanodiamonds compared to control cells was evaluated with laser scanning confocal microscopy (Figure 6D–F). Cell nuclei were counterstained (blue) in order to determine the cell locations. As can be seen in Figure 6D, the control cells only display the nuclear signal compared to the non-fluorescent well-purified DNDs (Figure 6E), which display weak background fluorescence compared to the strong areas of red fluorescence for the carbon-dot-decorated nanodiamonds (Figure 6F). These images suggest that fluorescent CDD-ND are indeed well-suited for in vitro cell culture imaging.

2.3.2. Polymer Nanocomposites

Figure S8 (Supporting Information) illustrates photographs of a cellulose composite containing CDD-ND (left) and a pure cellulose film (right) on a glass slide. Red luminescence imparted by the CDD-ND to the film is clearly seen at the bottom left picture.

3. Discussion

In this work, we have demonstrated that during treatment of detonation soot in a 3:1 mixture of sulfuric and nitric acids, luminescent composite structures consisting of NDs decorated

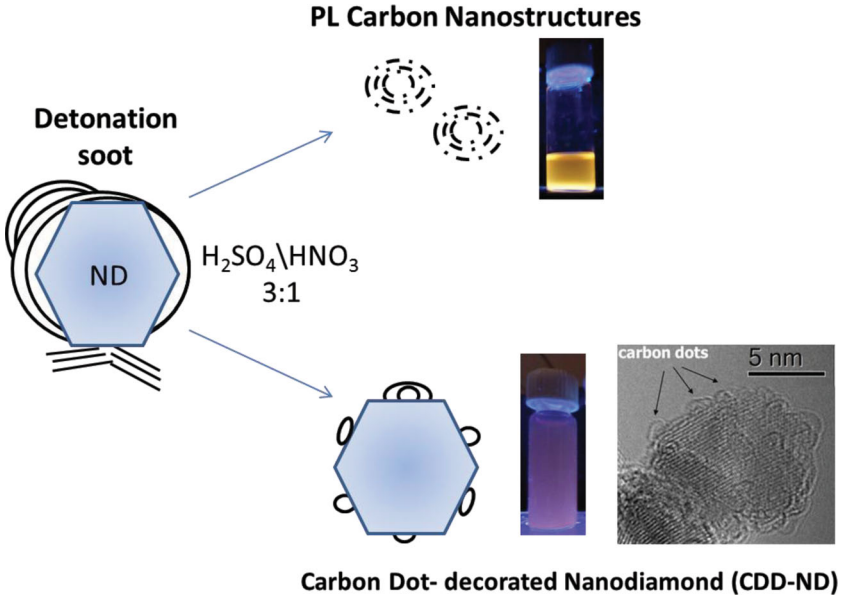

Figure 7. Schematic of the formation of PL products by treatment of detonation soot in a mixture of 3:1 sulfuric/nitric acid:carbon dots decorated ND produced from the diamond phase of the detonation soot (bottom) and free standing PL nanocarbon structures including carbon balls (Figure 3b), formed by oxidation of the non-diamond carbon in the soot (top).

with 1–2 nm rounded nanocarbon particles can be produced (**Figure 7**). These rounded structures, permanently attached to the ND surface, are 1–2 atomic layers thick, highly defected graphitic structures. Two important conditions for the production of CDD-ND are (1) the use of detonation soot as a starting material and (2) a 3:1 sulfuric/nitric acid mixture as an oxidizer. This mixture of sulfuric and nitric acids is a known graphite intercalating reagent,[42,43] which penetrates between the graphitic planes resulting in expansion of the planes, followed by oxidation and breaking of extended graphitic structures. It has also been shown that the dilation and the oxidation of graphitic carbon is most efficient when using a 3:1 ratio of sulfuric/nitric acids,[42] proving to be a highly efficient method to produce tiny nanometer-sized oxidized graphitic/graphene structures.[35,44]

During synthesis by detonation of explosives, ND is formed by crystallization of liquid carbon droplets when the temperature and pressure correspond to the ND phase region in the nanocarbon phase diagram[23]; when the pressure drops below the diamond–graphite equilibrium, the growth of diamond is replaced by the formation of graphite on the surface of ND particles as well as in the surrounding area. As a result, the nanodiamond lattice forms covalently bound structures with surrounding graphitic regions. If cooling of the detonation products is not performed fast enough, a fraction of the NDs is converted into OLC during synthesis (Figure 3a). During controlled etching of non-diamond carbon using GIC acids, graphitic structures are efficiently oxidized and destroyed around the ND particles, but for a certain period of time, tiny graphitic spots remain attached to the ND surface. The conditions of the treatment in a mixture of sulfuric/nitric acids can be chosen to avoid complete etching of non-diamond carbon structures from ND surfaces.

Simultaneously with the formation of CDD-ND, free-standing carbon spheres, 5–10 nm in size, are formed by the oxidation of the non-diamond carbon in the soot (Figure 7, top). These structures possess very bright luminescence and can be used as PL structures on their own, when extracted from the reaction medium. Thus, the present approach allows production of PL structures from both diamond and non-diamond carbon components of the detonation soot. The rounded or semispherical, well-separated 1–2 nm sp^2 carbon structures reported in this work are clearly different from the sp^2 carbon layers and cage structures, seen in HRTEM images of typical DND[41,45] and do not resemble bucky-shells on (111) surfaces[46] either.

CDD-NDs possess orange-red PL, which is more than 20 times brighter than the intrinsic PL observed for well-purified DND (Figure 2), which is attributed to the surface defects.[30] As we have shown above, in the CDD-ND composite PL is mainly attributed to the PL of the carbon dots permanently attached to the ND surface. To date, a plethora of different types of ultrasmall (few nms) carbon-based structures with bright luminescence had been produced.[12–14] Numerous mechanisms of the PL emission were suggested, mostly based on the presence of surface energy trapping sites.[12–14] Defected graphitic structures of the rounded carbon dots on the ND surfaces and the presence of carboxylic acid groups suggest a possible mechanism of emission based upon an electronic coupling of carboxylic acid groups with nearby atoms in polycylic aromatic compound-like species.[22] Unique features of the current carbon dots structures are, however, related to their tiny size, approximately 1–2 nm in diameter, smaller than the sizes of typical carbon and graphene dots.[12–14] Another peculiarity is their predominant red-NIR emission. A shift of the PL emission into the orange region was observed when the duration of the acid treatment was increased. This shift can be explained in terms of a size-dependent blue-shift, related to bandgap electron transitions in QDs.[14] However, carbon dots on ND surfaces quickly oxidize and eventually disappear, so that yellow or shorter wavelength emission was not revealed. This is possibly connected with the fact that ≈1 nm carbon dot structures providing red emission are mechanically stable on the ND surface, whereas smaller structures that would provide shorter wavelength emission are not mechanically stable. It cannot be excluded that the red-NIR positions of the PL could be related to interaction of the carbon dots with the NDs (either with its surface or interior optically active defects). Further studies are therefore required to explain the PL properties of the diamond–carbon dots composites. Importantly, through correct choice of the duration and temperature of the acid treatment, a maximum position and intensity of CDD-ND PL in the red-NIR regions can be obtained (Figure 2).

It is interesting that these highly PL structures were not observed previously, as the 3:1 sulfuric/nitric acid treatment is

Part. Part. Syst. Charact. **2014**,
DOI: 10.1002/ppsc.201300251

quite popular for ND purification and carboxylation.[47] Within the detonation ND community, there is a method of oxidation of non-diamond carbon in the detonation soot through treatment of the soot with a mixture of concentrated nitric and sulfuric acids (often with addition of sulfur anhydride) at temperatures exceeding 250 °C for several hours.[48] The conditions of treatment described in Brylyakov et al.[48] correspond to complete removal of non-diamond carbon from the DND surface, which is considered standard practice in producing high-purity nanodiamonds. However, in our method, the process of refluxing at lower temperatures with careful control of reaction time allows control of the amount of non-diamond carbon left on DND surfaces, resulting in the appearance of PL properties.

4. Conclusion

In this paper, we report a simple and efficient method for the production of ND-based, all-carbon, highly PL structures. The produced CDD-ND structures were fractionated down to a 20–30 nm size fraction. There is however no fundamental limit to the production of 5 nm primary CDD-ND, by disintegration of the ND aggregates within detonation soot through the use of, e.g., bead milling prior to the acid treatment. The high luminescence of the all-carbon CDD-ND composites, which are water stable due to the oxygen-containing groups at the particle surfaces, can be used in a wide variety of applications. As demonstrated in the cell study in the present work, CDD-ND with their predominant red-NIR emission, are attractive biolabels for in vitro cell culture imaging. It can be, in principle, considered for in vivo imaging in small animal studies. Nanodiamonds have been extensively studied as potential injectable therapeutic agents for generalized drug delivery in mouse models of cancer,[49] where carboxylated detonation NDs were shown to be drug carriers with a high loading capacity. Nanocarriers imaging capability is an important aspect of the in vivo studies, which was achieved in ref.[49] by conjugating detonation ND with a NIR dye. CDD-ND can further extend the potential of detonation ND as a drug carrier by providing intrinsic red-NIR imaging capability, eliminating need in NIR dyes, and a carboxylated surface, preferable for binding of a broad range of therapeutics.[49]

CDD-ND can be also valuable research tools in the development of DND-based polymer nanocomposites, as they can allow visualization of DND distribution within a polymer matrix and facilitate the development of the nanocomposite processing. As NDs are nanoadditives that can significantly improve mechanical properties of composites and coatings, CDD-ND provide a new functionality to nanocomposites, fluorescence. Their production cost can, in principle, be comparable to the cost of typical DND, opening perspectives for large-scale applications in PL nanocomposites, cosmetics, optoelectronics, photovoltaic, and anti-counterfeiting products.

5. Experimental Section

Starting Material: Detonation soot (sample soot-1) provided by SKN, Russia, was produced by detonation of a mixture of TNT/RDX in ice cooling media. Sample soot-2 was provided by NPO Altai, Russia, and was synthesized in a mixture of TNT/RDX in CO_2 cooling media. Theses samples were synthesized in the so-called "wet" and "dry" cooling conditions, correspondingly. The soot-1 contains ≈70 wt% of nanodiamond and soot-2 about 35% of nanodiamond. Soot samples were purified from metallic impurities by treatment in HCl. Final incombustible impurities content in both samples was about 1 wt%.

Oxidation Reaction: An amount of 250 mg of detonation soot was added to a 200-mL three-neck round bottom flask, along with 50 mL mixture of a three to one ratio of 95%–98% sulfuric acid (Aldrich) and 68% nitric acid (J.T. Baker). The flask was fitted with a water-cooled reflux condenser and a thermometer. The gas evolved was neutralized by bubbling through a solution of sodium hydroxide. Using an oil bath, the bath temperature was elevated to the appropriate temperature (between 90 and 120 °C) while the mixture was stirred. After the mixture was heated for different time intervals (from 15 min to 24 h) at the appropriate temperature, the flask was allowed to cool to room temperature. During reaction, probes of the reaction media were collected at different time intervals. After cooling, the residue was collected by centrifugation at 5000–20 000*g* forces for 10 min and washed with deionized (DI) water until the supernatant had a value above pH 5. At this stage, transparent supernatant after collection of the CDD-ND residue did not show any photoluminescence, indicating that free standing carbon dots were completely removed by washing. Then washing was continued until the CDD-ND had acquired a high negative zeta potential (at least −35 mV) and at least part of NDs remained suspended in DI water after the centrifugation at 25 000*g* forces. The residue for XRD, XPS, and Raman spectroscopy characterization was dried overnight under vacuum at 50 °C.

Luminescence Measurements: PL spectra of the powders were recorded at room temperature using a LABRAM HR spectrometer with 488 nm excitation light from an Ar+ laser. The laser beam was focused at a spot 2 μm in diameter on the surface of the CDD-ND samples. The PL of the sample was too high to be able to record Raman spectra.

The PL spectra of suspensions were recorded at room temperature using a laser Raman spectrometer with 488 nm excitation light from an Ar+ laser. The output power was 400 mW, and the real power density in cuvette was 10 W cm^{-2} at 488 nm excitation. For suppression of the elastic scattering, an edge filter (Semrock) was used. It allowed measurement of spectra separated by 100 cm^{-1} from the laser excitation. The system of registration consisted of monochromator (Acton, grades 900 and 1800 grooves mm^{-1}, focal length 500 nm, spectral resolution 1 cm^{-1}) and two detectors: PMT (Hamamatsu, H-8259-01) and a CCD camera (Jobin Yvon, Synapse1024* 128 BIUV-SYN).

PL stability of aqueous suspensions of typical DND, CDD-ND, nanoGO, and Alexa of the same concentration 0.3 g L^{-1} has been studied. The cuvette with solutions was fixed in a cuvette holder for 2 h, being constantly irradiated with laser radiation at 488 nm wavelength. Spectra were recorded with PMT every 15 min in the range from 500 to 800 nm. The geometry of the experiment and experimental conditions was identical for all the solutions. The obtained curves were corrected for laser power, signal accumulation time, PMT sensitivity, sample absorption.

Transmission Electron Microscopy: To prepare the samples, a drop of a water-based CDD-ND solution was placed on a carbon-coated copper grid and left to dry. Bright-field TEM and electron diffraction experiments were carried out on a Philips CM30 microscope, operated at 300 kV. High-resolution TEM, STEM, and spatially resolved EELS experiments were carried out on a FEI Titan 80-300 "cubed" microscope fitted with an aberration-corrector for the imaging lens and the probe forming lens, an electron monochromator and a GIF Quantum energy filter for spectroscopy, operated at 80 kV to minimize knock-on damage to the sample. For high-resolution imaging, the electron monochromator was used to provide an energy resolution of ≈0.3 eV, doing so extending the information transfer in the HRTEM images. STEM-EELS experiments were performed using a convergence semi-angle α of ≈21 mrad and a collection semi-angle β of ≈24 mrad, at a beam current of approximately 80 pA. A fine electron probe (diameter ≈1.5 Å) was scanned over a region of the sample, acquiring an EELS spectrum at each point. All

spectra were acquired at an energy dispersion of 0.25 eV per pixel and an energy resolution of approximately 1.2 eV. Chemical maps for the C signals (non-diamond carbon and diamond) were generated by fitting the carbon K-edge to a known reference for diamond and the internal reference for non-diamond carbon (bottom spectrum Figure 5).

Cell Studies: The human keratinocyte cell line (HaCaT) was purchased from the American Type Culture Collection (ATCC). The cells were cultured in T-75 flasks with RPMI 1640 cell culture media (Invitrogen) supplemented with 10% fetal bovine serum (ATCC) and 1% penicillin/streptomycin (Sigma), and incubated at 37 °C in a humidified incubator with 5% CO_2. For nanodiamond exposure, the RPMI 1640 media was supplemented with 1% penicillin/streptomycin and no serum. HaCat cells were plated at ≈350 000 cells mL^{-1} in two-chambered slides and allowed to adhere and grow for 24 h prior to dosing with nanodiamonds. Non-fluorescent DND and fluorescent nanodiamonds (CDD-ND) were incubated with human keratinocyte (HaCat) cells in culture in order to determine if their PL is strong enough to be useful for cell biology in vitro studies. Both forms of nanodiamonds were probe-tip sonicated for 1 min (20W, Cole-Palmer instrument), then diluted to final dosing concentrations of 25 μg mL^{-1} in cell culture media.

Transmitted light microscope images of live cells after 24 h of dosing with NDs were taken on an Olympus IX71 inverted phase contrast microscope and were captured via QCapture Pro Imaging Software. Fluorescent images were taken on a BD Pathway laser scanning confocal microscope with Attovision 5 software at 20× magnification after fixation of the cells and counterstaining of the nuclei with SYTOX Green dye (Invitrogen, false colored blue) followed by preservation with Prolong Gold Antifade reagent (Invitrogen).

Formation of Cellulose/CDD–ND Composite: CM-Cellulose (Sigma) was dissolved in 1 mL of DI water in the amount of 5 wt%. Then, 1 mL of 0.25 wt% CDD-ND water suspension was added and the mixture was sonicated, cast on a glass slide and dried overnight at room temperature. Resulting cellulose-CDD-ND nanocomposites contained 5% of CDD-ND.

Supporting Information

Supporting Information is available from the Wiley Online Library or from the author.

Acknowledgements

Financial support was provided in part by the Space and Naval Warfare Systems Centers (SSC) under Grant N66001-04-1-8933, Russian Foundation for Basic Research grants 08-02-01306, 08-05-00745, and 12-01-31523_mol_a, by the Federal Program of the Russian Ministry of Education and Science, grant 8398, the European Union Framework 7 program under Program No. 262348 (European Soft Matter Infrastructure (ESMI)), the ERC grant "Countatoms" and the fund for scientific research Flanders (FWO post-doctoral grant S.T.). The Titan electron microscope used for this research was partially funded through the Hercules Foundation of the Flemish government. We acknowledge assistance of Eugene Shenderov and Zaynab Mahbooba with experiments. Thanks to Dr. Laura Braydich-Stolle for assistance with the laser scanning confocal microscope. A.M.S. received funding from the National Research Council (NRC) Fellowship program funded by the Joint Science and Technology Office for Chemical and Biological Defense (JSTO-CBD), a program administered by the Defense Threat Reduction Agency (DTRA). S.T. gratefully acknowledges the Fund for Scientific Research Flanders (FWO). I.I.V. acknowledges partial funding of this work from RFBR grant no. 13-02-12434, President's grant for leading scientific schools no. 3076.2012.2, from Russian Academy of Sciences, program no. 24.

Received: July 21, 2013
Revised: October 11, 2013
Published online :

[1] R. Duncan, R. Gaspar, *Mol. Pharm.* **2011**, *8*, 2101.
[2] M. Freebody, *Photonics Spectra* **2013**, February, 42.
[3] X. Michalet, F. F. Pinaud, L. A. Bentolila, J. M. Tsay, S. Doose, J. J. Li, G. Sundaresan, A. M. Wu, S. S. Gambhir, S. Weiss, *Science* **2005**, *307*, 538.
[4] N. Lewinski, V. Colvin, R. Drezek, *Small* **2008**, *4*, 26.
[5] J. M. Klostranec, W.C. Chan, *Adv. Mater.* **2006**, *18*, 1953.
[6] B. Mahler, P. Spinicelli, S. Buil, X. Quelin, J. P. Hermier, B. Dubertret, *Nat. Nanotech.* **2008**, *7*, 659.
[7] X. Wang, X. Ren, K. Kahen, M. A. Hahn, M. Rajeswaran, S. Maccagnano-Zacher, J. Silcox, G. E. Cragg, A. L. Efros, T. D. Krauss, *Nature* **2009**, *459*, 686.
[8] J. Fan, P.K. Chu, *Small* **2010**, *6*, 2080.
[9] A. M. Edmonds, M. A. Sobhan, V. K. A. Sreenivasan, E. A. Grebenik, J. R. Rabeau, E. M. Goldys, A. Zvyagin, *Part. Part. Syst. Characterization* **2013**, *30*, 506.
[10] Y.Z. Lu, W. Chen, *Chem. Soc. Rev.* **2012**, *41*, 3594.
[11] J. Zheng, C. Zhou, M. Yu, J. Liu, *Nanoscale* **2012**, *4*, 4073.
[12] J. H. Liu, S. T. Yang, X. X. Cheng, H. Wang, *Curr. Drug Metabolism* **2012**, *13*, 1046.
[13] S. Zhu, S. Tang, J. Zhang, B. Yang, *Chem. Commun.* **2012**, *48*, 4527.
[14] L. Cao, M. Maziani, S. Sahu, Y. P. Sun, *Acc. Chem. Res.* **2013**, *46*, 171.
[15] Y.-P. Sun, B. Zhou, Y. Lin, W. Wang, K. A. S. Fernando, P. Pathak, M. J. Meziani, B. A. Harruff, X. Wang, H. Wang, P. G. Luo, H. Yang, M. E. Kose, B. Chen, L. M. Veca, S.-Y. Xie, *J. Am. Chem. Soc.* **2006**, *128*, 7756.
[16] X. Zhang, S. Wang, C. Zhu, M. Liu, Y. Ji, L. Feng, L. Tao, Y. Wei, *J. Colloid. Interface Sci.* **2013**, *397*, 39.
[17] P. X. Anilkumar, L. Wang, S. Cao, J. Sahu, P. Liu, K. Wang, L. Korch, A. Tackett, A. Parenzan, Y.-P. Sun, *Nanoscale* **2011**, *3*, 2023.
[18] X. Sun, Z. Liu, K. Welsher, J. T. Robinson, A. Goodwin, S. Zaric, H. Dai, *Nano Res.* **2008**, *1*, 203.
[19] G. Eda, Y.-Y. Lin, C. Mattevi, H. Yamaguchi, H.-A. Chen, I.-S. Chen, C.-W. Chen, M. Chowalla, *Adv. Mater.* **2010**, *22*, 505.
[20] J. Shen, Y. Zhu, C. Chen, X. Yang, C. Li, *Chem. Commun.* **2011**, *47*, 2580.
[21] T. Gokus, R. R. Nair, A. Bonetti, M. Bohmler, A. Lombardo, K. S. Novoselov, A. K. Geim, A. C. Ferrari, A. Hartschuh, *ACS Nano* **2009**, *3*, 3963.
[22] C. Galande, A. D. Mohite, A. V. Naumov, W. Gao, L. Ci, A. Ajayan, H. Gao, A. Srivastava, R. B. Weisman, P. M. Ajayan, *Oxid. Sci. Rep.* **2011**, *1*, 85.
[23] V. N. Mochalin, O. Shenderova, D. Ho, Y. Gogotsi, *Nat. Nanotech.* **2012**, *7*, 11.
[24] Y.-R. Chang, H.-Y. Lee, K. Chen, C.-C. Chang, D.-S. Tsai, C.-C. Fu, T.-S. Lim, Y.-K. Tzeng, C.-Y. Fang, C.-C. Han, H.-C. Chang, W. Fann, *Nat. Nanotech.* **2008**, *3*, 284.
[25] T. L. Wee, Y. W. Mau, C. Y. Fang, *Diamond Relat. Mater.* **2009**, *18*, 567.
[26] S. Yu, M. Kang, H. Chang, K. Chen and Y. Yu, *J. Am. Chem. Soc.* **2005**, *127*, 17604.
[27] C.-C. Fu, H.-Y. Lee, K. Chen, *Proc. Natl. Acad. Sci. USA* **2007**, *104*, 727.
[28] Nanodiamonds: Applications in Biology and Nanoscale Medicine (Ed:D. Ho), Springer, New York **2010.**
[29] O. A. Shenderova, I. I. Vlasov, S. Turner, G. Van Tendeloo, S. B. Orlinskii, A. A. Shiryaev, A. A. Khomich, S. N. Sulyanov, F. Jelezko, J. Wrachtrup, *J. Phys. Chem. C* **2011**, *115*, 14014.
[30] I. I. Vlasov, O. Shenderova, S. Turner, O. I. Lebedev, A .A. Basov, I. Sildos, M. Rahn, A. A. Shiryaev, G. Van Tendeloo, *Small* **2010**, *6*, 687.
[31] E. Osawa, *Diamond Relat. Mater.* **2007**, *16*, 2018.
[32] V. Mochalin, Y. Gogotsi, *J. Am. Chem. Soc.* **2009**, *131*, 4594.

[33] O. Shenderova, S. C. Hens, I. Vlasov, V. Borjanovic, G. McGuire, *Mater. Res. Soc. Symp. Proc.* **2010**, *1203*, 1203-J08-01.
[34] S. C. Hens, G. Cunningham, G. McGuire, O. Shenderova, *Nanosci. Nanotechnol. Lett.* **2011**, *3*, 75.
[35] S. C. Hens, W. G. Lawrence, A. S. Kumbhar, O. Shenderova, *J. Phys. Chem. C.* **2012**, *116*, 20015.
[36] O. Shenderova, I. Vlasov, S. A. C. Hens, V. Borjanovic (International Technology Center), US Patent Application 20100181534(International Technology Center), *US Patent Application 20100181534* **2010**.
[37] V. L. Kuznetsov, A. L. Chuvilin, Y. V. Butenko, I. Y. Malkov, V. M. Titov, *Chem. Phys. Lett.* **1994**, *222*, 343.
[38] T. A. Dolenko, S. A. Burikov, J. M. Rosenholm, O. A. Shenderova, I. I. Vlasov, *J. Phys. Chem.* **2012**, *116*, 24314.
[39] D. N. Klyshko, V. V. Fadeev, *Sov. Phys. Dokl.* **1978**, *23*, 55.
[40] R. F. Egerton, Electron Energy-Loss Spectroscopy in the Electron Microscope, 3rd ed. Springer, New York **2011**.
[41] S. Turner, O. I. Lebedev, O. Shenderova, I. I. Vlasov, J. Verbeeck, G. Van Tendeloo, *Adv. Funct. Mater.* **2009**, *19*, 2116.
[42] V. V. Avdeev, N. E. Sorokina, N. V. Maksimova, I. Y. Martnynov, A. V. Sezemin, *Inorg. Mater.* **2001**, *37*, 366.
[43] M. S. Dresselhaus, G. Dresselhaus, *Adv. Phys.* **2002**, *51*, 1.
[44] J. Peng, W. Gao, B. K. Gupta, Z. Liu, R. Romero-Aburto, L. H. Ge, L. Song, L. B. Alemany, X. B. Zhan, G. H. Gao, *Nano Lett.* **2012**, *12*, 844.
[45] V. L. Kuznetsov, I. L. Zilberberg, Y. V. Butenko, A. L. Chuvilin, B. Segall, *J. Appl. Phys.* **1999**, *86*, 863.
[46] J. Y. Raty, G. Galli, *Nat. Mater.* **2003**, *2*, 792.
[47] L. C. L. Huang, H. C. Chang, *Langmuir* **2004**, *20*, 5879.
[48] P. M. Brylyakov, P. P. Sataev, T. M. Gubarevich, A. K. Ladonina, N. G. Bruleva, A. M. Pavlov, M. A. Dimidova,*Patent SU 1794888* **1993**.
[49] E. K. Chow, X. Q. Zhang, M. Chen, R. Lam, E. Robinson, H. Huang, D. Schaffer, E. Osawa, A. Goga, D. Ho, *Sci. Transl. Med.* **2011**, *3*, 73ra21.